



# **Journal of Geophysical Research: Atmospheres**

# **RESEARCH ARTICLE**

10.1002/2015JD024100

#### **Kev Points:**

- The terrestrial aridity responses to anthropogenic BC and SO<sub>4</sub> aerosols with CESM simulations
- BC leads to a global decrease in aridity index (drying) of 1.9%/°C
- SO<sub>4</sub> cooling leads to a modest decrease in aridity index 0.4% (drying) per °C cooling

#### **Correspondence to:**

L. Lin, lzulinlei@126.com

#### Citation:

Lin, L., A. Gettelman, Y. Xu, and Q. Fu (2016), Simulated responses of terrestrial aridity to black carbon and sulfate aerosols, *J. Geophys. Res. Atmos.*, *121*, 785–794, doi:10.1002/2015JD024100.

Received 17 AUG 2015 Accepted 30 DEC 2015 Accepted article online 5 JAN 2016 Published online 27 JAN 2016

# Simulated responses of terrestrial aridity to black carbon and sulfate aerosols

L. Lin<sup>1,2</sup>, A. Gettelman<sup>2</sup>, Y. Xu<sup>2</sup>, and Q. Fu<sup>1,3</sup>

<sup>1</sup>College of Atmospheric Sciences, Lanzhou University, Lanzhou, China, <sup>2</sup>National Center for Atmospheric Research, Boulder, Colorado, USA, <sup>3</sup>Department of Atmospheric Sciences, University of Washington, Seattle, Washington, USA

**Abstract** Aridity index (AI), defined as the ratio of precipitation to potential evapotranspiration (PET), is a measure of the dryness of terrestrial climate. Global climate models generally project future decreases of AI (drying) associated with global warming scenarios driven by increasing greenhouse gas and declining aerosols. Given their different effects in the climate system, scattering and absorbing aerosols may affect AI differently. Here we explore the terrestrial aridity responses to anthropogenic black carbon (BC) and sulfate (SO<sub>4</sub>) aerosols with Community Earth System Model simulations. Positive BC radiative forcing decreases precipitation averaged over global land at a rate of 0.9%/°C of global mean surface temperature increase (moderate drying), while BC radiative forcing increases PET by 1.0%/°C (also drying). BC leads to a global decrease of 1.9%/°C in AI (drying). SO<sub>4</sub> forcing is negative and causes precipitation a decrease at a rate of 6.7%/°C cooling (strong drying). PET also decreases in response to SO<sub>4</sub> aerosol cooling by 6.3%/°C cooling (contributing to moistening). Thus, SO<sub>4</sub> cooling leads to a small decrease in AI (drying) by 0.4%/°C cooling. Despite the opposite effects on global mean temperature, BC and SO<sub>4</sub> both contribute to the twentieth century drying (AI decrease). Sensitivity test indicates that surface temperature and surface available energy changes dominate BC- and SO<sub>4</sub>-induced PET changes.

#### 1. Introduction

Terrestrial aridity depends on precipitation (P) and the evaporative demand of the atmosphere. The latter can be represented by potential evapotranspiration (PET), which can be estimated by the common Penman-Monteith equation [Penman, 1948; Monteith, 1981]. The aridity index (AI) is a measure of the dryness of terrestrial climate [ $Middleton\ and\ Thomas$ , 1992; Arya, 2001], which is defined by the ratio of annual P to annual PET. AI is a better metric of aridity than either P or PET alone. AI accounts for climate factors and has been used to examine future aridity changes [ $Sherwood\ and\ Fu$ , 2014]. The United Nations Convention to Combat Desertification [ $United\ Nations\ Convention\ to\ Combat\ Desertification$ , 1994] classifies dry lands by AI < 0.65 and further divides dry lands into hyperarid (AI < 0.05), arid (0.05 < AI < 0.2), semiarid (0.2 < AI < 0.5), and dry subhumid (0.5 < AI < 0.65) regions [ $Middleton\ and\ Thomas$ , 1992; Hulme, 1996; Mortimore, 2009].

Many climate models project 21st century drying over land [Feng and Fu, 2013; Cook et al., 2014; Scheff and Frierson, 2015; Lin et al., 2015; Zhao and Dai, 2015]. Using the Coupled Model Intercomparison Project Phase 5 (CMIP5) transient CO2 increase simulations [Taylor et al., 2012], Fu and Feng [2014] showed that the P averaged over land increases by 1.4% per degree of global mean surface air temperature increase, while PET increases at 4.6%/°C, leading to an Al decrease (i.e., drying) by 2.9%/°C. Combining observational and reanalysis data for 1948–2008, Feng and Fu [2013] revealed that global dry lands have expanded in the last 60 years. Basing on the data compiled by Feng and Fu [2013], Huang et al. [2015] found that the largest expansion of dry lands has occurred in semiarid regions since the early 1960s. Regionally, Li et al. [2015] also found a significant expansion of dry lands in northern China between 1948–1962 and 1994–2008. Using the historical observation, Gao et al. [2015] show that half of the stations in the semiarid northwestern Tibetan Plateau became drier between 1979 and 2011. Nastos et al. [2013] showed that drier conditions are expected in many regions of Greece at the end of the 21st century.

Using three sets of ensemble simulations from the Community Earth System Model (CESM) (see details of these ensemble simulations in *Kay et al.* [2014], *Sanderson et al.* [2015], and *Xu et al.* [2015]), L. Lin et al. (Simulated differences in 21st century aridity due to different scenarios of greenhouse gases and aerosols, submitted to *Climatic Change*, 2015) showed that the normalized change in Al due to greenhouse gases (GHGs) agrees with Al changes due to  $CO_2$  alone [Fu and Feng, 2014], as  $CO_2$  is the largest forcing term among

©2016. The Authors.
This is an open access article under the terms of the Creative Commons
Attribution-NonCommercial-NoDerivs
License, which permits use and distribution in any medium, provided the original work is properly cited, the use is non-commercial and no modifications

or adaptations are made.



all GHGs in the 21st century. L. Lin et al., submitted manuscript, 2015 also showed that projected anthropogenic aerosol decreases in the 21st century have little impact on global land aridity because aerosols cause both a precipitation reduction and PET reduction. Thus, when both GHGs and aerosols are included, CO<sub>2</sub> remains the most important anthropogenic factor in determining the current and future changes in Al (Q. Fu et al., Changes in terrestrial aridity for the period 850–2080 from the Community Earth System Model, submitted to *Journal of Geophysical Research Atmospheres*, 2015). Similarly, *Zhao et al.* [2015] found that the effects of dust aerosols are indiscernible in the expansion of arid and semiarid areas using the Beijing Climate Center Atmospheric General Circulation Model version 2.0.1 [*Zhang et al.*, 2012; *Wu et al.*, 2010]. In this work we will expand on these earlier results to attempt to attribute the effects of aerosols on aridity (Al) by aerosol types.

The total aerosol effects on climate are highly uncertain [Boucher et al., 2013; Zhang et al., 2015]. Different types of aerosols can have different climate impacts because they affect the radiative budget differently. However, previous studies [L. Lin et al., submitted manuscript, 2015; Zhao et al., 2015] did not compare or contrast the effects of various aerosol types on aridity. Here we examine the aridity response to two prominent anthropogenic aerosol species: light-scattering sulfate (SO<sub>4</sub>) and light-absorbing black carbon (BC) using global climate model simulations driven by individual forcings. We also discuss the physical mechanisms of the model responses. This helps clarify and put into context earlier work.

#### 2. Methods

### 2.1. Model and Experiments

We use the Community Earth System Model (CESM) version 1 for this study. The climate simulated by CESM have been evaluated by *Meehl et al.* [2013] and *Lin et al.* [2015]. A comprehensive three-mode model aerosol module and two-moment bulk cloud microphysical scheme have been implemented in the model [*Morrison and Gettelman*, 2008; *Liu et al.*, 2012]. The direct and indirect effects of aerosols on clouds play an important role in climate change [*Gettelman et al.*, 2010; *Ghan et al.*, 2012]. Cloud droplet size is very important in the calculation of cloud radiation [*Zhang et al.*, 2010]. In particular, BC is an effective absorber of solar radiation (direct effect) with small impacts on cloud droplets. Sulfate aerosols reduce the short-wave radiation reaching to the surface by scattering, and by reducing total surface energy, also reduce global precipitation. Sulfate aerosols are also effective cloud condensation nuclei and ice nuclei for homogeneous freezing and they thus have a large impact on cloud droplet size, known as aerosol indirect effects [*Twomey*, 1977], that further brighten clouds and cool the climate by reflecting more solar radiation back to space.

CESM1 simulations are conducted using a fully coupled model with instantaneous forcing. The control case is a 394 year preindustrial simulation. Starting from the end of the 319th year, we ran two simulations, each with a single forcing change for another 75 years, with the last 60 years of output analyzed, allowing the first 15 years for model spin-up. The forcing is imposed by instantaneously increasing BC emissions or SO<sub>2</sub> emissions (a precursor of SO<sub>4</sub>) from preindustrial to present-day levels [Lamarque et al., 2011]. CO<sub>2</sub> and other GHG concentrations remain constant at preindustrial levels. This methodology is analogous to the classical instantaneous CO<sub>2</sub> doubling experiment [Manabe and Wetherald, 1975]. The long averaging time (60 years in the perturbed simulation versus 394 years for the preindustrial control simulations) enabled us to dampen the influence of decadal natural variability and to obtain a clear effect due to aerosol perturbation. Differences are shown as present minus preindustrial. This yields the effect of present-day aerosols. Additionally, we analyzed the simulations under an instantaneous increase of forcing of CO<sub>2</sub> (260 to 400 ppm) to put the results in context with previous studies that focused on GHG induced changes. These same simulations have also been used to study the response of mountain snowpack to CO<sub>2</sub> and aerosol forcing [Xu et al., 2015].

To increase the signal-to-noise ratio for BC (due to a smaller BC forcing), an ensemble of five perturbed simulations were conducted. Present-day BC emissions are adjusted from the standard emission inventory to account for the potential underestimation of BC emissions. The standard emission inventories are from *Lamarque et al.* [2010], BC emission increases since 1850 are mostly located in regions of the Northern Hemisphere (NH) (e.g., China and India). Emissions over East Asia are increased by a factor of 2 and South Asia by 4. BC emissions were adjusted in all sectors (energy, industrial, etc.) and all seasons by the same ratio. *Xu et al.* [2013] showed that such an adjustment would improve model simulated radiative forcing compared with values derived from observations. Without the adjustments, the modeled forcing (and simulated temperature change) would be lower by about a factor of 2 to 4 [*Xu et al.*, 2013]. However, since we will normalize



Table 1. The Normalized Change (Scaled by Global Mean Surface Air Temperature Change) of Surface Air Temperature (SAT), Precipitation (P), Potential Evapotranspiration (PET), Aridity Index (AI), Surface Relative Humidity (RH), Available Energy (Rn-G), Net Downward Long-Wave Radiation (Rn,I), Net Downward Short-Wave Radiation (Rn,s), and Wind Speed  $(u_2)$  Averaged Over Land  $(60^{\circ}\text{S to }90^{\circ}\text{N})^{a}$ 

	SAT (°C/°C)	P (%/°C)	PET (%/°C)	AI (%/°C)	RH (%/°C)	Rn-G (W m $^{-2}$ °C $^{-1}$ )	Rn,I (Wm $^{-2}$ °C $^{-1}$ )	Rn,s (W m $^{-2}$ °C $^{-1}$ )	$u_2 (10^{-2} \text{ms}^{-1} {}^{\circ}\text{C}^{-1})$
ВС	$1.6 \pm 0.2$	$-0.9 \pm 2.4$	1.0 ± 1.4	$-1.9 \pm 3.7$	$-1.0 \pm 0.5$	$-3.7 \pm 1.1$	0.1 ± 1.0	$-3.8 \pm 1.7$	0.1 ± 1.4
$SO_4$	$1.5 \pm 0.1$	$6.7 \pm 1.5$	$6.3 \pm 0.4$	$0.4 \pm 1.6$	$-0.5 \pm 0.2$	$3.5 \pm 0.4$	$-1.4 \pm 0.3$	$4.9 \pm 0.5$	$0.1 \pm 0.6$
CO <sub>2</sub>	$1.2 \pm 0.04$	$1.2 \pm 0.4$	$4.6 \pm 0.2$	$-3.3 \pm 0.5$	$-0.9 \pm 0.1$	$1.3 \pm 0.1$	$0.5 \pm 0.2$	$0.8 \pm 0.1$	$-0.3 \pm 0.2$
GHGs	$1.3 \pm 0.03$	$1.7 \pm 0.5$	$4.9 \pm 0.2$	$-2.7 \pm 0.6$	$-0.8 \pm 0.1$	$1.4 \pm 0.1$	$0.6 \pm 0.1$	$0.7 \pm 0.1$	$0.2 \pm 0.2$
Aerosols	$1.5 \pm 0.1$	$6.1 \pm 1.7$	$6.4 \pm 0.6$	$0.1 \pm 1.9$	$-0.3 \pm 0.3$	$3.7 \pm 0.3$	$-0.2 \pm 0.4$	$3.9 \pm 0.4$	$-0.3 \pm 0.4$

<sup>&</sup>lt;sup>a</sup>The changes due to greenhouse gases (GHGs) and total aerosols obtained from L. Lin et al. (submitted manuscript, 2015) are shown for comparison. Noted that the SO<sub>4</sub> radiation forcing is negative forcing and induced global mean temperature change is negative (cooling). The uncertainty range is one standard deviation.

the responses by surface temperature change, the enhancement will not affect the results but serve to increase the signal-to-noise ratio.

PET is computed from available energy (Rn-G), surface air temperature (SAT), relative humidity (RH), and 2 m wind speed  $(u_2)$  using the Food and Agriculture Organization Penman-Monteith method [Allen et al., 1998]. Monthly output is used in the equation, and  $u_2$  is derived from the  $u_{10}$  (10 m wind speed) output using the equation given by Allen et al. [1998]. For details, see L. Lin et al. (submitted manuscript, 2015).

#### 3. Results

#### 3.1. Global Mean Values

Table 1 lists the global land average change of SAT, P, PET, AI, and other key parameters as the difference between the control and perturbed simulations with increased BC, SO<sub>4</sub>, and CO<sub>2</sub>. Values are scaled by the respective changes in global mean surface air temperature (°C). The scaling is used here because the CO<sub>2</sub> forcing is 2 to 4 times larger than the other aerosol forcings, and in this study, we are interested in the mechanism of AI change, not the absolute value of the changes. The latter is more model and scenario dependent. The results due to all GHGs and all aerosols from L. Lin et al. (submitted manuscript, 2015) are also shown for comparison. To evaluate the uncertainties associated with internal variability, we divide the last 60 years of perturbed simulations to four 15 year periods and contrast this to four 15 year periods from the control run. We do this in all combinations of the four periods (differencing each 15 period of perturbation to each 15 period of the control) to generate a standard deviation from 16 differences. The mean is similar to the mean of 60 year differences. The same method for assessing uncertainty is also used in Figures 3 and 3.

The scaled changes in SAT due to BC and SO<sub>4</sub> are similar (1.6°C/°C and 1.5°C/°C, respectively). Note that the change in SAT associated with SO<sub>4</sub> is negative. Per one degree of global mean temperature change, the land mean temperature changes by 1.6 for BC and 1.5° for SO<sub>4</sub>, partly due to a larger aerosol forcing associated with their primary emission sources over land than over ocean. A warming over land is also seen in CO<sub>2</sub> cases (1.2°C/°C) but to a smaller extent. The land-ocean contrast in CO<sub>2</sub>-driven warming is also observed in other global climate models [e.g., Joshi et al., 2008]. The main explanation is that the drier land boundary layer will generally warm more than the ocean boundary layer in order to maintain a neutral stability in the atmosphere [Joshi et al., 2008], while the reduction of land relative humidity also plays a role in contributing to larger land warming [Byrne and O'Gorman, 2013]. However, the spatially inhomogeneous radiative forcing from aerosols leads to more localized temperature responses (e.g., higher land-ocean warming ratio) than CO<sub>2</sub> despite moderating effects of the ocean (Xu et al., Understanding the spatial patterns of climate response to CO<sub>2</sub>, sulfate and black carbon aerosols in a global climate model, in preparation for Journal of Climate). The aerosol contribution also helps explain why the land-ocean warming ratio has larger model-to-model differences than GHG forcing in twentieth century simulations compared to 21st century simulations because the radiative forcing in the twentieth century simulations has a larger aerosol component [Joshi et al., 2013].

The scaled land precipitation changes, however, are of different sign for BC (-0.9%/°C) and SO<sub>4</sub> (6.7%/°C) forcing. Anthropogenic  $SO_4$  is a negative forcing that induces surface cooling and reduces precipitation. This results from lowering the incident energy to the surface. BC on the other hand causes surface warming and a small precipitation reduction in CESM. We investigate the mechanisms further below. The BC forcing result is consistent with results from Ming et al. [2010] that absorbing aerosols cause a net reduction in global

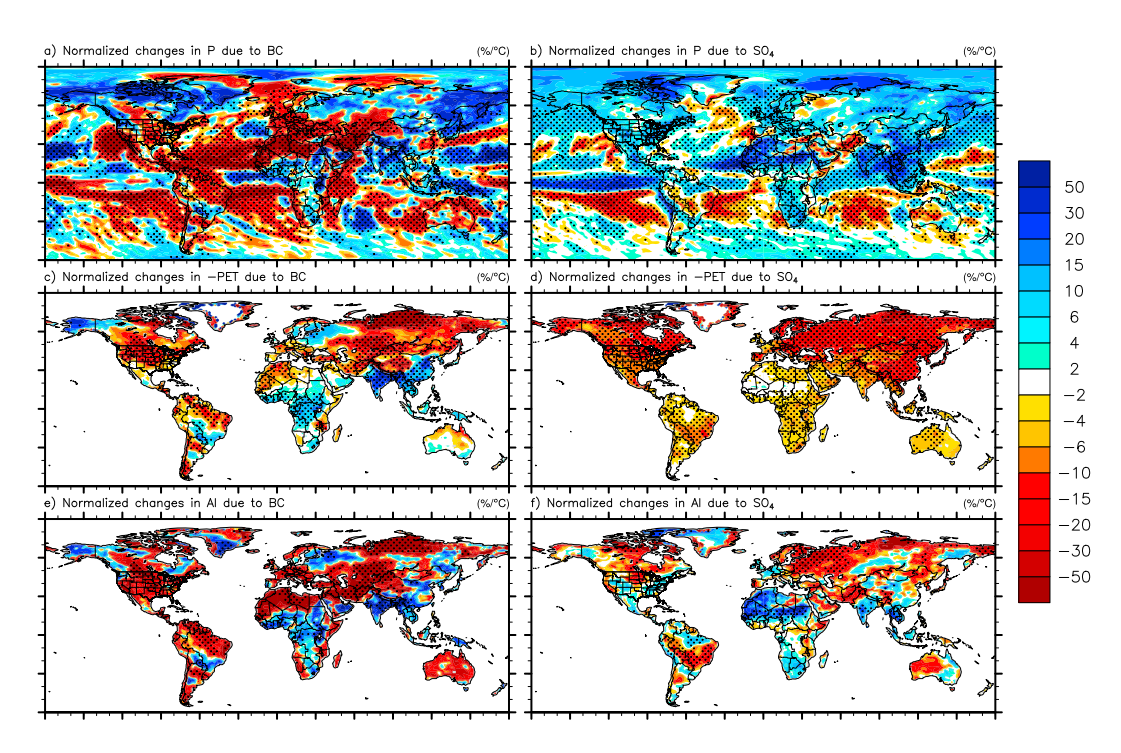


**Figure 1.** Changes in (a, b) precipitation (P), (c, d) potential evapotranspiration (PET), and (e, f) aridity index (Al) due to black carbon (Figures 1a, 1c, and 1e) and sulfate (Figures 1b, 1d, and 1f) aerosol, scaled by global mean surface air temperature changes. Grid points are stippled for statistically significant changes based on a 90% confidence interval from a two-sided *t* test.

mean precipitation. Rotstayn et al. [2000] have shown a shift of NH precipitation southward with aerosols indirect forcing from  $SO_4$ , and an overall reduction in precipitation. So both  $SO_4$  and BC reduce precipitation but with opposite sign of the global surface temperature change.

The scaled percent changes in global precipitation, i.e., the percent global precipitation change per unit of global surface air temperature change (%/°C), is called as the hydrological sensitivity. *Ocko et al.* [2014] found that the global hydrological sensitivity due to  $SO_4$  is 2.4%°C, while that due to BC is -1.5%°C using the GFDL (Geophysical Fluid Dynamics Laboratory) climate model. In this study the global hydrologic sensitivity is 3.7%°C for  $SO_4$  and -1.1%°C for BC.

Anthropogenic BC and  $SO_4$  lead to a change in PET by 1.0%°C and 6.3%°C, respectively (more details in section 3.3). Note that BC is generally a positive direct forcing causing warming, while  $SO_4$  is a negative forcing causing cooling by both direct and indirect effects [Ghan et al., 2012]. Overall, BC increases lead to AI decrease (drying) at -1.9%°C, and  $SO_4$  increases also lead to AI decrease because of cooling effect. However, the scaled change in aridity index due to  $SO_4$  (i.e., 0.4%°C) is much smaller because of the cancelation of the effects between PET and P. The response to  $SO_4$  is similar to L. Lin et al.'s (submitted manuscript, 2015) analysis on total aerosols because  $SO_4$  is the largest contribution to total aerosol forcing.

For both BC and SO<sub>4</sub>, changes in short-wave radiation  $(-3.8\pm1.7 \, \text{W/m}^2/^{\circ}\text{C})$  and  $4.9\pm0.5 \, \text{W/m}^2/^{\circ}\text{C}$ , respectively) dominate over changes in long-wave radiation  $(0.1\pm1.0 \, \text{W/m}^2/^{\circ}\text{C})$  and  $-1.4\pm0.3 \, \text{W/m}^2/^{\circ}\text{C}$ , respectively). Interestingly, for CO<sub>2</sub>, the short-wave radiation change  $(0.8\pm0.1 \, \text{W/m}^2/^{\circ}\text{C})$  at the surface is still larger than the long-wave radiation change  $(0.5\pm0.2 \, \text{W/m}^2/^{\circ}\text{C})$ , suggesting the feedbacks through cloud changes. This is in line with a recent study that showed that the primary causes of top of the atmosphere energy imbalance in response to CO<sub>2</sub> increase are coming from short-wave radiation [Donohoe et al., 2014].

#### 3.2. Regional Patterns

Figure 1 shows the global distributions of normalized changes in P, —PET, and AI due to BC and SO<sub>4</sub>. The negative PET is used so blue colors denote wetter conditions in all panels. BC increases P in North Asia but reduces P in most of North and South America and leads to a northward shift of the Intertropical



Convergence Zone (ITCZ) (Figure 1a). Our BC results agree with *Roberts and Jones* [2004], *Wang and Magnusdottir*, 2006, and *Mahajan et al.* [2013] who found a northward shift of the ITCZ with BC forcing. SO<sub>4</sub> has a stronger impact on the precipitation over North Africa, India, and south China (Figure 1b). A recent multimodel assessment of precipitation responses to SO<sub>4</sub> concludes that a southward shift of the ITCZ is found across nearly all CMIP3 and CMIP5 models [*Hwang et al.*, 2013]. In our simulations, the spatial pattern of changes in P due to SO<sub>4</sub> (Figure 1b) is similar to that reported in *Hwang et al.* [2013].

Despite many studies devoted to estimating precipitation response to various aerosol types, the PET response to aerosols is rarely discussed. Based on our simulations, BC reduces PET strongly over India and south China (Figure 1c). Despite a local warming effect due to BC that tends to increase PET, the surface dimming effect of BC leads to the PET reduction (see next section). In addition, BC suppresses precipitation and increases PET over North and South America, North Africa, Europe, and Australia, resulting in stronger drying in those regions (decreasing Al in Figure 1e). Present-day SO<sub>4</sub> aerosols have a larger impact on Al over South America, Europe, North Africa, and India (Figure 1f). In general, the PET response pattern due to anthropogenic SO<sub>4</sub> (Figure 1d) is more spatially uniform than that due to BC (Figure 1c). A negative SO<sub>4</sub> radiative forcing decreases PET everywhere in Figure 1d. The difference is due to the fact that BC imposes compensating effects on PET (i.e., surface dimming and surface warming), therefore causing the close-to-zero response and sign differences in many regions. On the other hand, SO4 consistently reduces PET across all regions. Next we investigate further the different components of PET changes.

In the next section, we explore the physical mechanisms of the Al change to understand why these changes occur.

#### 3.3. Physical Mechanisms of PET and AI Responses

We use equation (1) to quantify the relative contributions of changes in temperature, relative humidity, wind speed, and available energy to the total percentage changes in PET over global land to explore why BC and  $SO_4$  impact PET differently. For example, in order to isolate the effect of the temperature change (SAT) on PET due to BC over land, we calculate the PET using SAT with the BC perturbation run but using the other factors (RH,  $u_2$ , and Rn-G) from the control run and then compare this with the PET calculated using the inputs all from control run. The Appendix A in *Fu and Feng* [2014] describes the details on the method of deriving the individual contributions. Figure 2 shows the global distribution of the individual contributions of changes in SAT, RH,  $u_2$ , and Rn-G to the total percentage change in PET due to BC and  $SO_4$ . RH changes play an important role in the BC-induced PET change in CESM over North and South America (Figure 2a). Wind speed changes, however, have no significant influence to PET (Figures 2c and 2d). Among these variables, SAT is the largest contributor of PET change over most of land area (Figures 2e and 2f). The available energy (Rn-G) is also significant contributor to the  $SO_4$  induce PET change (Figure 2h) but is highly uncertain in the BC-induced PET change (Figure 2g) due to competing effect of surface warming and surface dimming.

Figure 3 shows the individual contributions from various physical factors over global land. The results of all GHGs and all aerosols from L. Lin et al. (submitted manuscript, 2015) are also shown for comparison. The effects of SAT on scaled PET changes over land due to BC and  $SO_4$  are similar (3.7%/°C and 3.3%/°C, respectively). BC warming leads to a PET increase, and  $SO_4$  cooling leads to a PET decrease. However, the effects of Rn-G are of opposite sign (-3.5%/°C and 2.5%/°C, respectively) because BC warming is accompanied by a surface dimming. Therefore, BC-induced PET change is smaller (1.0%/°C) because of two compensating effects: surface warming and surface dimming. For  $SO_4$ , surface temperature cooling and surface dimming work together to reduce PET (6.3%/°C). Note that  $SO_4$  and BC represent two extreme types of aerosols in terms of the radiation budget and their temperature impact. For example, organic carbon and dust aerosols are partially absorbing (BC like) and partially reflecting ( $SO_4$  like), and their impact on PET will likely fall between the values calculated in this paper. Since the total aerosols consist of  $SO_4$ , BC, and other aerosols, the total aerosol impact on PET is dependent on the chemical composition of aerosols, which determines their direct scattering and/or absorption properties, as well as their hygroscopicity and ability to enhance cloud droplet and ice crystal nucleation.

Similarly, we can derive the individual contributions of changes in SAT, RH,  $u_2$ , Rn-G, and P to the total global percentage change in Al (Figure 4), as discussed in L. Lin et al. (submitted manuscript, 2015). The changes in SAT and RH due to BC lead to consistent Al decreases (drying: a negative sign in Figure 4), with only the Rn-G term leading to increasing Al with BC (wetting: positive sign in Figure 4). The combined result

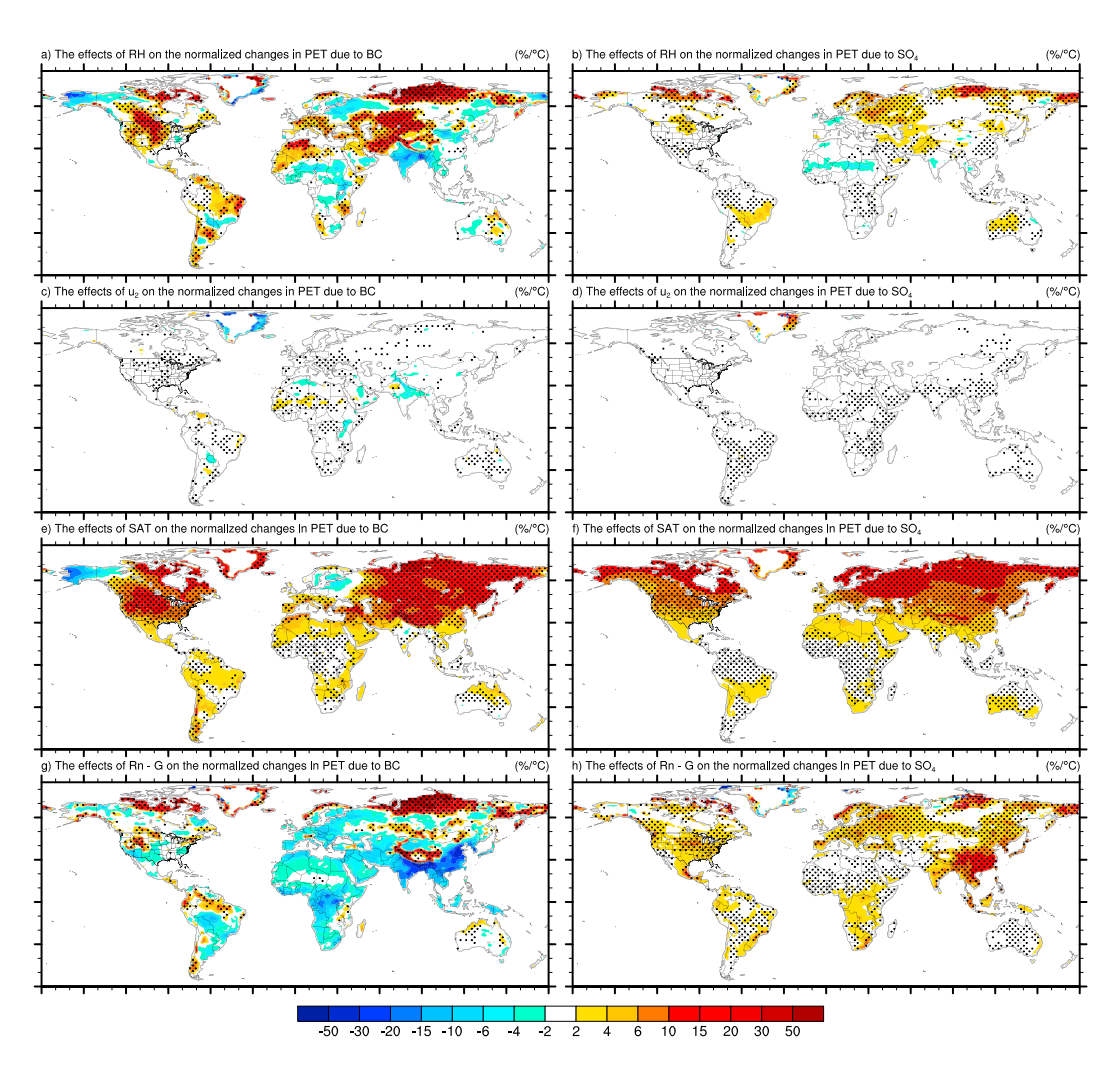
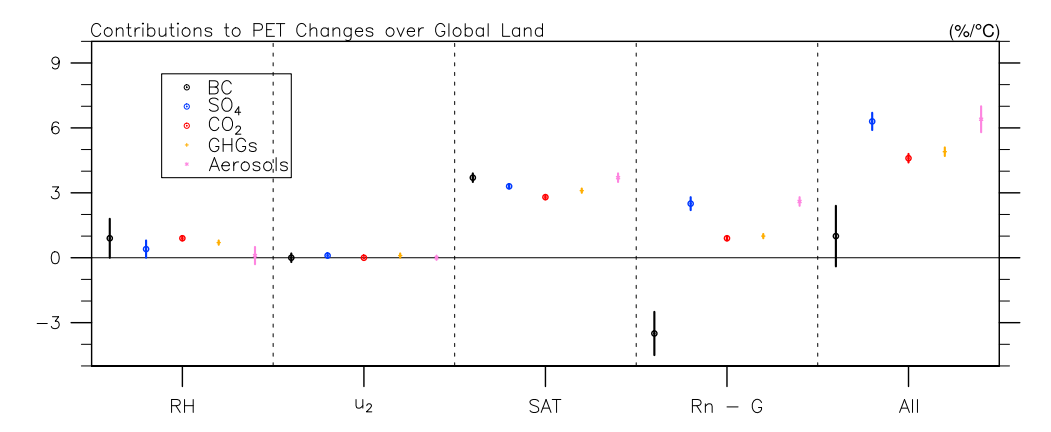
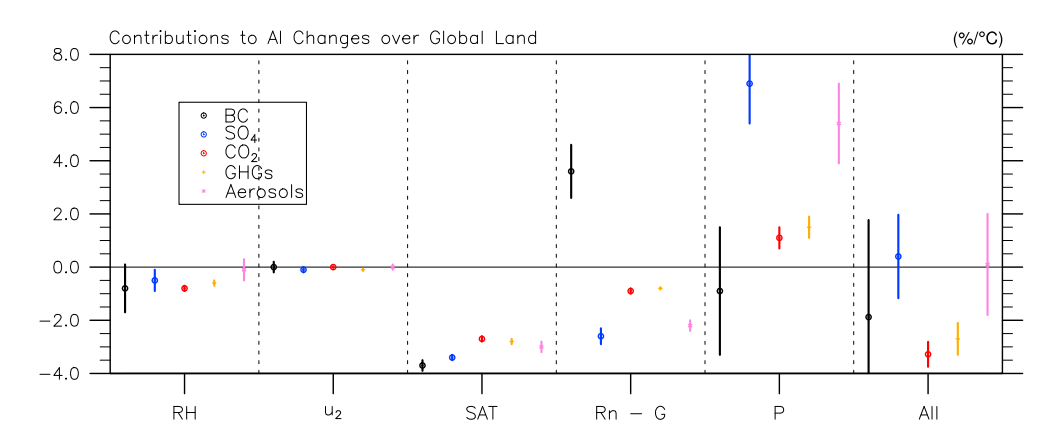


Figure 2. The effects (in percent change of PET per degree) of relative humidity (RH), wind speed  $(u_2)$ , surface air temperature (SAT), and available energy (Rn-G) on the percentage changes in PET due to black carbon aerosol and sulfate aerosol, scaled by global mean surface air temperature change. Grid points are stippled for statistically significant changes based on a 90% confidence interval from a two-sided t test.



**Figure 3.** The effects (in percent change of PET per degree) of relative humidity (RH), wind speed  $(u_2)$ , surface air temperature (SAT), and available energy (Rn-G) on the percentage changes in potential evapotranspiration (PET) over global land due to black carbon aerosol, sulfate aerosol, and  $CO_2$ , scaled by global mean surface air temperature change. The results of greenhouse gases (GHGs) and aerosols from L. Lin et al. (submitted manuscript, 2015) are shown for comparison. The error bar denotes two standard deviation.



**Figure 4.** The effects (in percent change of AI per degree) of relative humidity (RH), wind speed  $(u_2)$ , surface air temperature (SAT), available energy (Rn-G), and precipitation (P) on the percentage changes in aridity index (AI) over global land due to black carbon aerosol, sulfate aerosol, and  $CO_2$ , scaled by global mean surface air temperature change. The results of greenhouse gases (GHGs) and aerosols from L. Lin et al. (submitted manuscript, 2015) are shown for comparison. The error bar denotes two standard deviation.

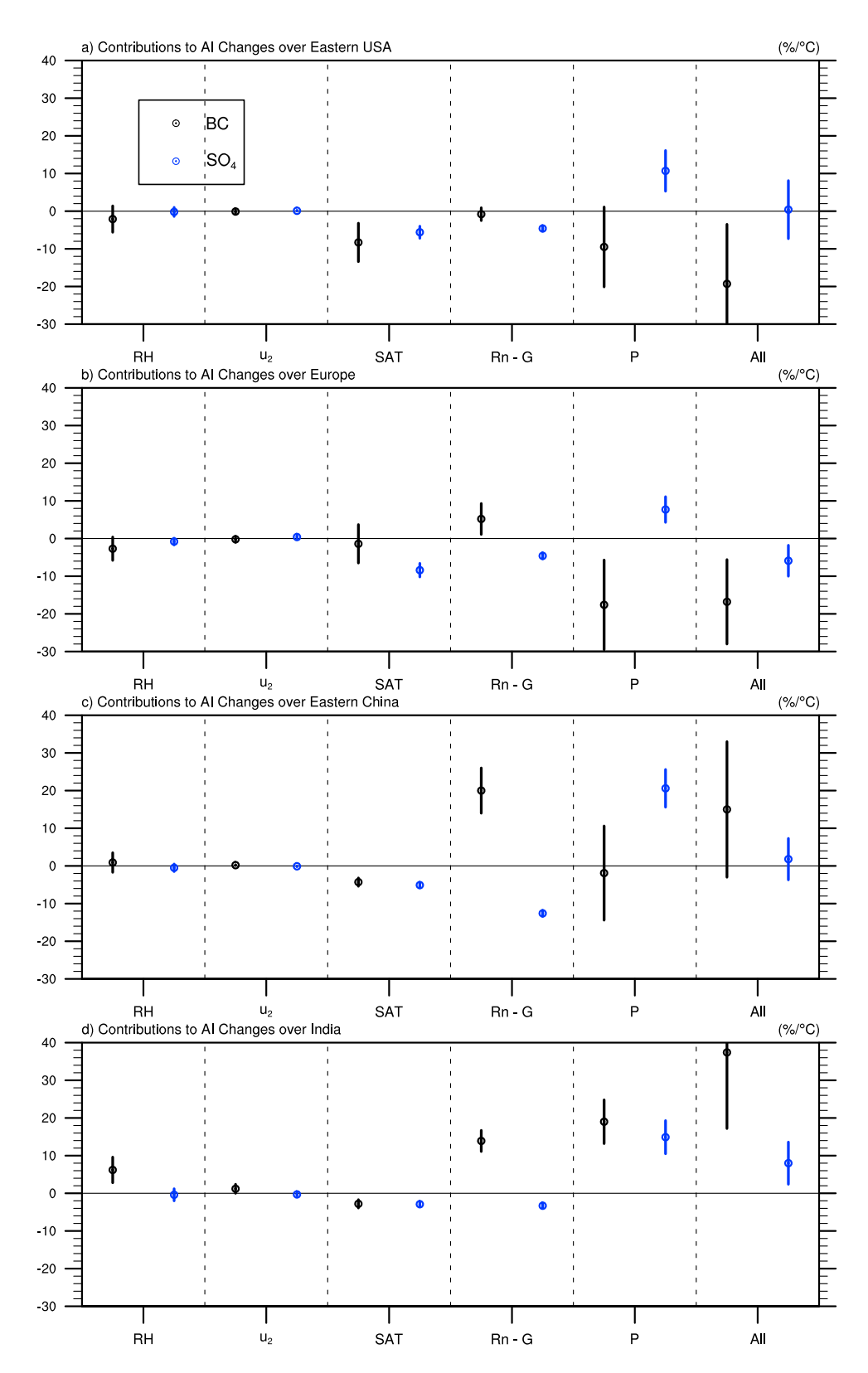
is a modest decrease in AI of -1.9%/°C for BC forcing. SAT and Rn-G are the biggest factors to BC-induced AI change (-3.7 and 3.6%/°C, respectively). In addition, the P response leads to a change AI of -0.9%/°C. For the negative SO<sub>4</sub> radiative forcing, the SO<sub>4</sub>-induced changes (normalized by temperature changes) in SAT and Rn-G lead to an AI change of -6.5%/°C, but this is almost completely offset by the P response (the latter leads to a change AI of 6.9%/°C for SO<sub>4</sub>).

Figure 5 illustrates the individual contributions of changes in SAT, RH,  $u_2$ , Rn-G, and P to the total percentage change in AI for different regions. The regions are eastern USA (30°N–47°N, 76°W–98°W), Europe (42°N–62°N, 0°E–30°E), eastern China (20°N–37°N, 104°E–121°E), and India (5°N–33°N, 60°E–90°E). Changes due to BC and SO<sub>4</sub> are shown separately. Aerosol-induced aridity changes are due to different factors across different regions (L. Lin et al., submitted manuscript, 2015). P changes dominate the SO<sub>4</sub> and BC-induced AI change in CESM over most regions. One exception is that available energy (Rn-G) dominates the aridity change due to BC in eastern China (Figure 5c). SAT is the largest contributor of the P/PET change due to SO<sub>4</sub> in Europe (Figure 5b). BC radiative forcing increases the aridity index (moistening) in eastern China and India (15.0%/°C and 37.5%/°C, respectively) while SO<sub>4</sub> cooling leads to an increase in AI (moistening) in Europe by 5.9%/°C cooling. Results indicate a leading role for precipitation, with a secondary role for available energy and surface temperature. Surface humidity and wind speed are not important for aerosol-induced aridity change.

## 4. Concluding Remarks

We have analyzed the effect on aridity using a series of simulations in CESM with two prominent anthropogenic absorbing and scattering aerosol species, black carbon (BC), and sulfate (SO<sub>4</sub>), respectively. Positive BC radiative forcing enhances the direct radiative heating of the atmosphere and increases the global mean surface air temperature. The atmospheric solar absorption due to BC suppresses P because less latent heat release is required to balance the atmospheric radiative cooling [O'Gorman et al., 2012]. However, based on the energy balance constraint on the hydrological cycle, the warming surface tends to increase the long-wave cooling that leads to a precipitation increase [Held and Soden, 2006]. Between these two competing factors, the suppression of P due to atmospheric absorption by BC outweighs the surface warming effects of BC, at least in CESM, resulting in a net decrease in the global mean precipitation due to BC. A similar result has been found for the GFDL model [Ocko et al., 2014] but with a slightly different magnitude. The results could be model dependent and especially sensitive to the altitude of BC layer in the model. On the contrary, SO<sub>4</sub> induces a significant land mean precipitation reduction (6.7%/°C), mainly due to surface cooling. The SO<sub>4</sub> effect seems consistent across models [Hwang et al., 2013].

Using precipitation as the sole metric, one may conclude that  $SO_4$  is more effective in causing drought than BC. Our study, however, revealed BC is more effective in causing aridity increases (decreasing AI, drier), when also considering the effects of PET changes. The mechanisms are summarized as follows: BC decreases the



**Figure 5.** The effects (in percent change of AI per degree) of relative humidity (RH), wind speed  $(u_2)$ , surface air temperature (SAT), available energy (Rn-G), and precipitation (P) on the percentage changes in aridity index (AI) over eastern USA (30°N-47°N, 76°W-98°W), Europe (42°N-62°N, 0°E-30°E), eastern China (20°N-37°N, 104°E-121°E), and India (5°N-33°N, 60°E-90°E) due to black carbon aerosol and sulfate aerosol, scaled by global mean surface air temperature change. The error bar denotes two standard deviation.



solar radiation that reaches the surface, leading to a decrease of PET. On the other hand, BC-induced surface warming tends to increase PET. Interestingly, the surface warming due to BC outweighs the radiation in affecting PET, resulting in a net increase in the global mean PET, which lowers AI (increasing aridity) in addition to reducing P. Overall, BC leads to a -1.9%/°C Al change (drying).

 $SO_4$  however has smaller impact on Al (0.4%/°C). Note that the negative sulfate forcing decreases the global mean temperature, leading to a smaller AI (drying). This smaller impact on AI is because of the cancelation effects between P (6.7%/°C) and a PET (-6.3%/°C). The large change of PET is due to both the decreased solar radiation that reaches the land as well as the cooler surface temperature.

The conclusion that BC is a more effective drying agent (decreasing Al) than SO<sub>4</sub> (per unit surface temperature change) is based on the normalized calculation in the form of %/°C, because we aim to understand the physical mechanism of the changes. SO<sub>4</sub> twentieth century forcing is much larger than BC, and so the total effect for SO<sub>4</sub> is much larger, and therefore, SO<sub>4</sub> is still the main contributor among all aerosol species to the changes of hydrological cycle and aridity. This study using twentieth century aerosol forcing reaffirms our previous study (L. Lin et al., submitted manuscript, 2015) using 21st century forcing scenarios: aerosol-induced drying in terms of aridity index is much smaller than that estimated using precipitation alone. Aerosol effects are not just important for anthropogenic emissions, and this analysis may also have important implications for interpreting paleoclimate records associated with volcanic eruptions (Q. Fu et al., submitted manuscript, 2015). The volcanic SO<sub>4</sub> in the stratosphere may dry the land less than previously assumed because PET decreases may counteract much of the P decreases due to temperature, although there will be no indirect effects (due to a lack of clouds in the stratosphere). Our results suggest improving aerosol treatment in climate models and examinations of their roles in hydrological cycle are crucial for projection of future aridity. Future research using output from multiple models is needed to confirm the robustness of our results with CESM.

#### Acknowledgments

The authors thank Aixue Hu for helpful comments. This study is in part supported by the NSFC grants 41521004, 41275070, and 41405010, National Basic Research Program of China (2012CB955303), and the Fundamental Research Funds for the Central Universities (Izujbky-2015-k02). Y. Xu acknowledges supports from U.S. Department of Energy's Office of Science (BER, DE-FC02-97ER62402) and Advanced Study Programme (ASP) postdoctoral fellowship. Computing resources were provided by the Climate Simulation Laboratory at NCAR's Computational and Information Systems Laboratory, sponsored by the National Science Foundation and other agencies. The National Center for Atmospheric Research is supported by the U.S. National Science Foundation. For data requests, please contact the corresponding author (lzulinlei@126.com).

### References

Allen, R. G., L. S. Pereira, D. Raes, and M. Smith (1998), Crop evapotranspiration—Guidelines for computing crop water requirements-FAO Irrigation and drainage paper 56 FAO, Rome, 300, 6541.

Arya, P. S. (2001), Introduction to Micrometeorology, vol. 79, Academic Press, London.

Boucher, O., et al. (2013), Clouds and aerosols, in Climate Change 2013: The Physical Science Basis. Contribution of Working Group I to the Fifth Assessment Report of the Intergovernmental Panel on Climate Change, edited by T. F. Stocker et al., pp. 571-657, Cambridge Univ. Press, Cambridge, U. K., and New York.

Byrne, M. P., and P. A. O'Gorman (2013), Link between land-ocean warming contrast and surface relative humidities in simulations with coupled climate models, *Geophys. Res. Lett.*, 40, 5223–5227, doi:10.1002/grl.50971.

Cook, B. I., J. E. Smerdon, R. Seager, and S. Coats (2014), Global warming and 21st century drying, Clim. Dyn., 43(9-10), 2607-2627, doi:10.1007/s00382-014-2075-v.

Donohoe, A., K. C. Armour, A. G. Pendergrass, and D. S. Battisti (2014), Shortwave and longwave radiative contributions to global warming under increasing CO2, Proc. Natl. Acad. Sci. U.S.A., 111, 16,700-16,705.

Feng, S., and Q. Fu (2013), Expansion of global drylands under a warming climate, Atmos. Chem. Phys., 13(19), 10,081-10,094, doi:10.5194/ acp-13-10081-2013.

Fu, O., and S. Feng (2014), Responses of terrestrial aridity to global warming, J. Geophys. Res. Atmos., 119, 7863–7875, doi:10.1002/ 2014JD021608.

Gao, Y., X. Li, L. R. Leung, D. Chen, and J. Xu (2015), Aridity changes in the Tibetan Plateau in a warming climate, Environ. Res. Lett., 10(3), 034013. Gettelman, A., X. Liu, S. J. Ghan, H. Morrison, S. Park, A. J. Conley, S. A. Klein, J. Boyle, D. L. Mitchell, and J.-L. F. Li (2010), Global simulations of ice nucleation and ice supersaturation with an improved cloud scheme in the Community Atmosphere Model, J. Geophys. Res., 115, D18216, doi:10.1029/2009JD013797.

Ghan, S. J., X. Liu, R. C. Easter, R. Zaveri, P. J. Rasch, J. H. Yoon, and B. Eaton (2012), Toward a minimal representation of aerosols in climate models: Comparative decomposition of aerosol direct, semidirect, and indirect radiative forcing, J. Clim., 25(19), 6461-6476.

Held, I. M., and B. J. Soden (2006), Robust responses of the hydrological cycle to global warming, J. Clim., 19, 5686-5699.

Huang, J., M. Ji, Y. Xie, S. Wang, Y. He, and J. Ran (2015), Global semi-arid climate change over last 60 years, Clim. Dyn., 1–20, doi:10.1007/ s00382-015-2636-8.

Hulme, M. (1996), Recent climatic change in the world's drylands, Geophys. Res. Lett., 23, 61-64, doi:10.1029/95GL03586.

Hwang, Y. T., D. M. Frierson, and S. M. Kang (2013), Anthropogenic sulfate aerosol and the southward shift of tropical precipitation in the late 20th century, Geophys. Res. Lett., 40, 2845–2850, doi:10.1002/grl.50502.

Joshi, M. M., J. M. Gregory, M. J. Webb, D. M. Sexton, and T. C. Johns (2008), Mechanisms for the land/sea warming contrast exhibited by simulations of climate change, Clim. Dyn., 30(5), 455-465.

Joshi, M. M., F. H. Lambert, and M. J. Webb (2013), An explanation for the difference between twentieth and twenty-first century land-sea warming ratio in climate models, Clim. Dvn., 41(7-8), 1853-1869.

Kay, J., et al. (2014), The Community Earth System Model (CESM) large ensemble project: A community resource for studying climate change in the presence of internal climate variability, Bull. Am. Meteorol. Soc., 96, 1333-1349, doi:10.1175/BAMS-D-13-00255.1.

Lamarque, J. F., et al. (2010), Historical (1850–2000) gridded anthropogenic and biomass burning emissions of reactive gases and aerosols: Methodology and application, Atmos. Chem. Phys., 10(15), 7017-7039.

Lamarque, J. F., G. P. Kyle, M. Meinshausen, K. Riahi, S. J. Smith, D. P. van Vuuren, A. J. Conley, and F. Vitt (2011), Global and regional evolution of short-lived radiatively-active gases and aerosols in the representative concentration pathways, Clim. Change, 109(1), 191-212.



- Li, Y., J. Huang, M. Ji, and J. J. Ran (2015), Dryland expansion in northern China from 1948 to 2008, Adv. Atmos. Sci., 32(6), 870–876. Lin, L., A. Gettelman, S. Feng, and Q. Fu (2015), Simulated climatology and evolution of aridity in the 21st century, J. Geophys. Res. Atmos., 120, 5795–5815, doi:10.1002/2014JD022912.
- Liu, X., et al. (2012), Toward a minimal representation of aerosols in climate models: Description and evaluation in the Community Atmosphere Model CAM5. *Geosci. Model Dev.*. 5. 709–739.
- Mahajan, S., K. J. Evans, J. J. Hack, and J. E. Truesdale (2013), Linearity of climate response to increases in black carbon aerosols, *J. Clim.*, 26(20), 8223–8237.
- Manabe, S., and R. T. Wetherald (1975), The effects of doubling the CO2 concentration on the climate of a general circulation model, J. Atmos. Sci., 32, 3–15.
- Meehl, G. A., W. M. Washington, J. M. Arblaster, A. Hu, H. Teng, J. E. Kay, A. Gettelman, D. M. Lawrence, B. M. Sanderson, and W. G. Strand (2013), Climate change projections in CESM1 (CAM5) compared to CCSM4, J. Clim., 26(17), 6287–6308.
- Middleton, N., and D. Thomas (1992), in *World Atlas of Desertification: United Nations Environmental Programme*, edited by N. Middleton, D. S. G. Thomas and Edward Arnold, London.
- Ming, Y., V. Ramaswamy, and G. Persad (2010), Two opposing effects of absorbing aerosols on global-mean precipitation, *Geophys. Res. Lett.*, 37, L13701, doi:10.1029/2010GL042895.
- Monteith, J. L. (1981), Evaporation and surface temperature, Q. J. R. Meteorol. Soc., 107, 1–27.
- Morrison, H., and A. Gettelman (2008), A new two-moment bulk stratiform cloud microphysics scheme in the Community Atmosphere Model, version 3 (CAM3). Part I: Description and numerical tests, J. Clim., 21(15), 3642–3659.
- Mortimore, M. (2009), Dryland opportunities IUCN, Gland, Switzerland, HED, London, U. K., and UNDP, New York,
- Nastos, P. T., N. Politi, and J. Kapsomenakis (2013), Spatial and temporal variability of the Aridity Index in Greece, *Atmos. Res.*, *119*, 140–152. O'Gorman, P. A., R. P. Allan, M. P. Byrne, and M. Previdi (2012), Energetic constraints on precipitation under climate change, *Surv. Geophys.*, 33(3–4), 585–608, doi:10.1007/s10712-011-9159-6.
- Ocko, I. B., V. Ramaswamy, and Y. Ming (2014), Contrasting climate responses to the scattering and absorbing features of anthropogenic aerosol forcings, *J. Clim.*, 27(14), 5329–5345.
- Penman, H. L. (1948), Natural evaporation from open water, bare soil and grass, *Proc. R. Soc. London, 193A*, 120–145, doi:10.1098/rspa.1948.0037.
- Roberts, D. L., and A. Jones (2004), Climate sensitivity to black carbon aerosol from fossil fuel combustion, *J. Geophys. Res.*, 109, D16202, doi:10.1029/2004JD004676.
- Rotstayn, L. D., B. F. Ryan, and J. E. Penner (2000), Precipitation changes in a GCM resulting from the indirect effects of anthropogenic aerosols, *Geophys. Res. Lett.*, 27(19), 3045–3048, doi:10.1029/2000GL011737.
- Sanderson, B. M., K. W. Oleson, W. G. Strand, F. Lehner, and B. C. O'Neill (2015), A new ensemble of GCM simulations to assess avoided impacts in a climate mitigation scenario, *Clim. Change*, 1–16, doi:10.1007/s10584-015-1567-z.
- Scheff, J., and D. M. Frierson (2015), Terrestrial aridity and its response to greenhouse warming across CMIP5 climate models, J. Clim., 28, 5583–5600, doi:10.1175/JCLI-D-14-00480.1.
- Sherwood, S., and Q. Fu (2014), A drier future?, Science, 343(6172), 737-739.
- Taylor, K. E., R. J. Stouffer, and G. A. Meehl (2012), An overview of CMIP5 and the experiment design, *Bull. Am. Meteorol. Soc.*, 93(4), 485–498, doi:10.1175/bams-d-11-00094.1.
- Twomey, S. (1977), The influence of pollution on the shortwave albedo of clouds, J. Atmos. Sci., 34(7), 1149-1152.
- United Nations Convention to Combat Desertification (1994), U. N. Doc. A/A C. 241/27, 33 I. L. M. 1328, United Nations.
- Wang, C., and G. Magnusdottir (2006), The ITCZ in the central and eastern Pacific on synoptic time scales, *Mon. Weather Rev.*, 134(5), 1405–1421.
- Wu, T., R. Yu, and F. Zhang (2010), The Beijing Climate Center atmospheric general circulation model: Description and its performance for the present-day climate, *Clim. Dyn.*, *34*, 123–147, doi:10.1007/s00382-008-0487-2.
- Xu, Y., R. Bahadur, C. Zhao, L. Leung, and V. Ramanathan (2013), Estimating the radiative forcing of carbonaceous aerosols over California based on satellite and ground observations, *J. Geophys. Res. Atmos.*, 118, 11,148–11,160, doi:10.1002/jgrd.50835.
- Xu, Y., W. M. Washington, and V. Ramanathan (2015), Observed high-altitude warming and snow cover retreat over Tibet and the Himalayas enhanced by black carbon, *Atmos. Chem. Phys. Discuss.*, 15, 19,079–19,109, doi:10.5194/acpd-15-19079-2015.
- Zhang, H., F. Zhang, Q. Fu, Z. Shen, and P. Lu (2010), Two-and four-stream combination approximations for computation of diffuse actinic fluxes, *J. Atmos. Sci.*, 67(10), 3238–3252.
- Zhang, H., et al. (2012), Simulation of direct radiative forcing of aerosols and their effects on East Asian climate using an interactive AGCM-aerosol coupled system. Clim. Dyn., 38, 1675–1693, doi:10.1007/s00382-011-1131-0.
- Zhang, H., Z. Wang, F. Zhang, and X. Jing (2015), Impact of four-stream radiative transfer algorithm on aerosol direct radiative effect and forcing. *Int. J. Climatol.*. 35. 4318–4328.
- Zhao, S., H. Zhang, S. Feng, and Q. Fu (2015), Simulating direct effects of dust aerosol on arid and semi-arid regions using an aerosol–climate coupled system, *Int. J. Climatol.*, 35(8), 1858–1866.
- Zhao, T., and A. Dai (2015), The magnitude and causes of global drought changes in the 21st century under a low-moderate emissions scenario, J. Clim., 28, 4490–4512, doi:10.1175/JCLI-D-14-00363.1.